A robust subspace based approach to feedforward control of broadband disturbances on a novel six-degrees-of-freedom vibration isolation set-up

G. Nijsse, H. Super, J. Van Dijk and J.B. Jonker

University of Twente, Faculty of Engineering Technology

Department of Mechanical Engineering, Laboratory of Mechanical Automation

P.O. Box 217, NL-7500 AE, Enschede, The Netherlands

E-mail: {G.Nijsse, H.Super, J.VanDijk, J.B.Jonker}@CTW.UTwente.NL

May 4, 2005

Abstract

The contribution of this paper is twofold. First, the paper introduces a novel hybrid vibration isolation approach which uses a combination of passive and active vibration control techniques to provide additional design freedom. The approach can be used to meet higher design requirements with respect to vibration isolation. To illustrate the feasibility of the approach, a stiff hybrid six-degrees-of-freedom vibration isolation set-up will be presented. The objective of the set-up is to investigate if the receiver structure can be isolated from the source structure by six hybrid vibration isolation mounts, such that disturbances induced by the source structure are isolated from the receiver structure. Vibration isolation is established by minimizing signals from six acceleration sensor outputs and by steering six piezo-electric actuator inputs. Our second contribution is that a state space based fixed gain H_2 controller is designed, implemented and validated. Real-time broadband feedforward control results are presented (between 0 - 1 kHz) which show that an average reduction of

8.0 dB is achieved in the error sensor outputs in real-time.

Keywords: Active vibration isolation control, feedforward, hybrid, mount, state space, subspace, Wiener.

1 Introduction

Vibrations are an important issue in a wide range of engineering applications where mechanical parts need to be connected to each other and at the same time transfer of vibrations between the parts needs to be minimal. They can make machines less accurate, result in unwanted noise, can cause fatigue in parts of the structure or can even directly cause damage. Examples can be found in the area of precision technology, transport vehicles, space and aerospace technology and so on. Vibration isolation aims at reducing the transmission of vibration from one body or structure to another. The body where the vibration originates from and the structure on which this body is mounted are respectively called for short the ‘source’ and ‘receiver’. A rigid source needs to be connected to a receiver appropriately, in order to constrain the rigid body motions of the source relative to the receiver. Passive vibration isolation [Hansen and Snyder, 1997; Mead, 1998] by reducing the stiffness of the mounts between a vibrating source and a receiver construction is a well-known conventional technique to reduce the transfer of vibrations between them [Hansen and Snyder, 1997]. The stiffness of the mount determines the fundamental resonance frequencies of the mounted system. Vibrations with a frequency higher then this are attenuated. However, unfortunately other design requirements (like static stability) often impose a minimum allowable stiffness, thus limiting the achievable vibration isolation by passive means. In some cases active vibration isolation can be a solution [Hansen and Snyder, 1997; Elliott, 2000; Fuller et al., 1996]. Most six independent degrees-of-freedom (DOF) active vibration isolators found in literature are based on Stewart platforms (see e.g. [Horodinca et al., 2002; A. Abu Hanieh and Preumont, 1999]). In

this paper a new approach is presented which proposes a stiff and statically determined support by using hybrid (hard) mounts to facilitate both passive and active vibration isolation control. Specifically, the goal of this paper is twofold. It

- describes the hybrid vibration isolation approach applied to the design of a stiff hybrid 6DOF vibration isolation set-up consisting of three 2DOF hybrid mounts [Super et al., 2004].

- is investigated if a broadband disturbance can be rejected in the error sensor outputs of the set-up, by using a subspace based feedforward fixed gain H_2 controller [Nijsse et al., 1999; Elliott, 2000; Vidyasagar, 1985; Nijsse, Super, Dijk and Jonker, 2004]. In order to compute the controller, models are required of the transfer path between the:

  1. disturbance input and the error sensor outputs i.e. the primary path [Kuo and Morgan, 1996].
  2. actuator inputs and the error sensor outputs i.e. the secondary path.

  In this paper subspace model identification (SMI) is used to obtain state space models i.e. black box model identification based on input/output data (see [Nijsse, Dijk and Jonker, 2004]). Particularly, the past output multi-variable output error SMI routine is used [Verhaegen, 1994].

This paper is organized as follows. In section 2 the design of the 6DOF vibration isolation set-up is explained. In section 3 the prerequisites are treated concerning the control experiments. That is, the section gives the notation, introduces the problem statement and gives the controller design. In section 4 SMI is explained and the actual identification results are given. In section 5 the simulation and real-time control results are given. Finally, in section 6 conclusions are presented.

2 Design of the vibration isolation set-up

The hybrid approach can be used when a high stiffness mounting of the source on the receiver is required while still achieving vibration isolation for certain disturbances acting on the source. The basic idea is to

have the minimum required number of so-called hybrid paths for a stiff (static) support while preventing other - unwanted and unnecessary - paths between the source and receiver, which otherwise could result in unwanted vibration transfers. Here, a path is defined as a path along which vibration energy is transferred from the source to the receiver. A hybrid path contains an actuator and sensor for active vibration isolation control and should only provide high stiffness in the actuator (active) direction. The actuator is capable of nullifying the force transfer through the hybrid path for a certain dynamic disturbance force acting on the source when a correct steering signal is provided by the active vibration isolation controller. With this approach it is theoretically possible to provide complete vibration isolation for a disturbance while still having the benefits of a stiff passive support between the source and receiver which provides static support.

The remainder of this section discusses the design of the experimental vibration isolation set-up with a 6DOF source based on the hybrid vibration isolation approach. For this set-up three 2DOF hybrid mounts are used. Each mount is dominantly stiff in only two directions aligned with two actuators used for active vibration isolation control. Specifically, the following aspects are important for the design of the set-up based on the hybrid approach:

- **Only hybrid paths between source and receiver.** Important for the design is that every connection between the source and receiver should be either hybrid or provide sufficient passive vibration isolation. Passive paths in a hybrid vibration isolation system outside the hybrid directions can deteriorate the overall vibration isolation performance or, at worst, result in no vibration isolation at all. The presence of these so-called parasitic or flanking paths should - at best - be prevented. In practice this implies that their stiffness should be that low that it is able to provide sufficient passive isolation outside the hybrid directions. To be exact, due to the design of the construction of the three mounts, the transferred vibration energy can only be passed through the paths with dominant stiffness in which also is a actuator present: in total six paths.

- **Statically determined system.** Although - in theory - it should be possible to use more than six actuators and six error sensors for hybrid vibration isolation set-ups, it is still beneficial to opt for a statically determined design. For that reason preferably six independent 1DOF hybrid vibration isolation paths should be present, providing for the static stability for the 6DOF source.

- **2DOF mount concept.** Although a configuration based on a Stewart platform seems an obvious choice for 6DOF vibration isolation purposes, it is not convenient for many engineering applications e.g. to support an engine. Therefore, the choice was made for a configuration based on a 2DOF mount. As such, three of these mounts need to be placed between the source and the receiver.

- **Stiff mounting.** The stiffness between the source and the receiver is designed to be high compared to the more commonly found low stiffness vibration isolation solutions. This is to demonstrate the strength of this method: having a relative stiff static support in combination with sufficient vibration isolation performance for both narrowband and broadband disturbance signals.

A photograph of the setup is depicted in figure 1 on the left; a schematic picture is given on the right. A

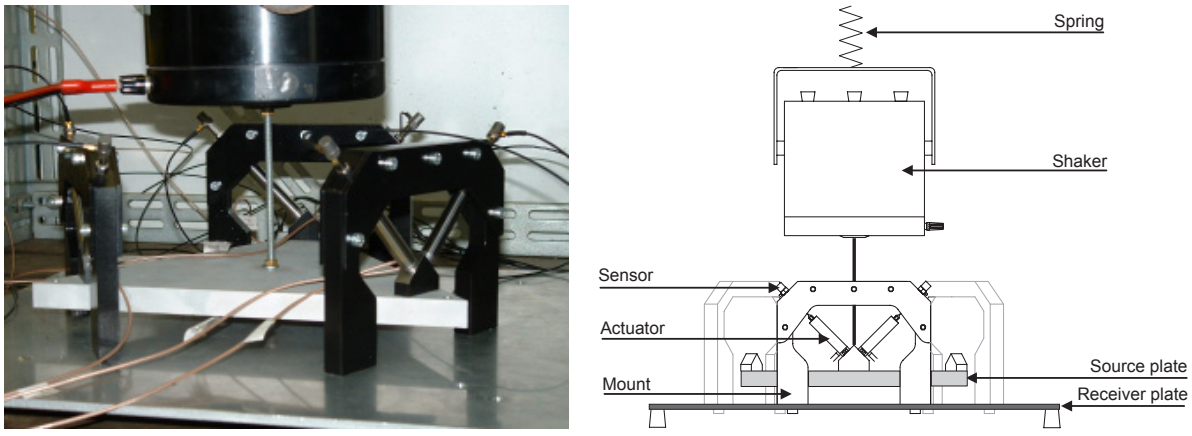

Figure 1: *A photo of the 6DOF vibration isolation set-up (left) and a schematic picture (right).*

Brüel & Kjaer 4809 vibration exciter (with 2706 power amplifier) excites the triangular aluminum source

plate (sides 260mm, thickness 15mm) in vertical direction. This vibrating source is mounted on a square receiver plate (400x400x5mm) by three hybrid mounts placed at angles of 120 degrees: each mount fixes 2DOF. Figure 2 shows one of the mounts in more detail. Both hybrid DOFs of the mount consist of a piezo-electric actuator fixed to the source of the mount. On the other end a slender flexible joint is mounted to prevent the transfer of shear forces and bending moments. This enables force transfer domi-

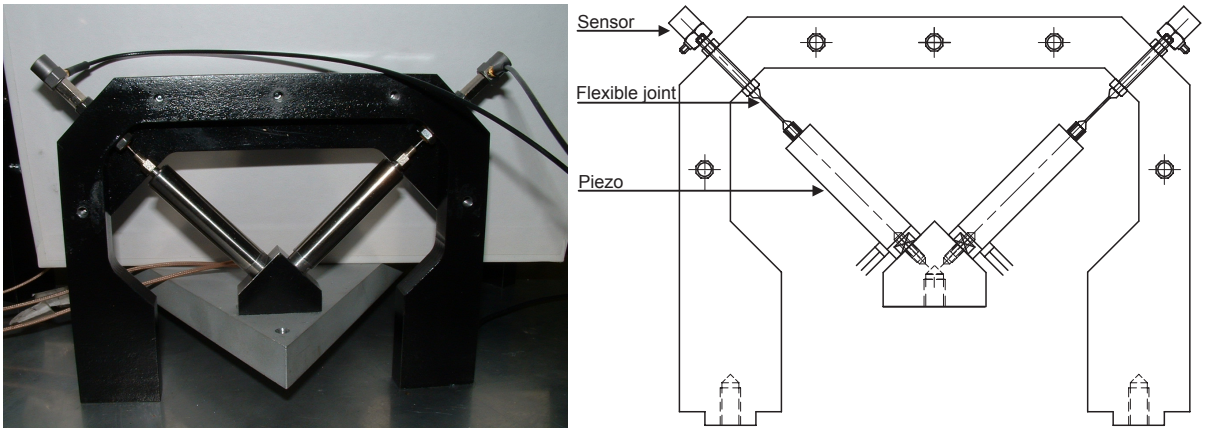

Figure 2: *Photograph (left) and schematic picture (right) of one mount (front plate removed) showing the two piezoelectric actuators, the (slender) flexible joints and the two sensors (accelerometers) at the corners of the mount.*

nantly in the working line (hybrid direction) of the actuator. As a consequence, stiffness in other than the hybrid directions results in so-called parasitic paths which deteriorate the achievable vibration isolation performance. The length and thickness of the joint has been chosen carefully to ensure sufficient compliance in those directions while maintaining sufficient stiffness in axial direction and prevent buckling of the joint. Note that the choice for a 'hanging' configuration creates a pre-tension force in the joints due to the weight load of the source plate, which gives an additional protection against buckling. The actuators used in the mount are mechanical pre-stressed PSt150/5/40 piezo-electric actuators [Fukuda and Tzou, 2002] from Piezomechanik with SVR 150/3 Piezomechanik power amplifiers. Accelerations in line with the actuators are being measured with Brüel & Kjaer 4393 accelerometers connected to Brüel

& Kjaer Nexus 2629 conditioning amplifiers, which also provides a low-pass (setting 1kHz) filtering on the sensor signals for anti-aliasing purposes. These six error sensor outputs are used by the controller. For data acquisition and controller implementation a dSPACE DS1005 digital signal processing board is being used (see also [Thoeni, 1994] for more information about real-time systems).

3 Notation, problem statement and controller design

This section is organized as follows. In section 3.1 the notation is given, while in section 3.2 the problem statement is posed and the controller design is given.

3.1 Notation

$\mathbf{Y}(q^{-1})$ is a linear time invariant transfer function with q^{-1} the unit delay operator. Often, $\mathbf{Y}(q^{-1})$ is abbreviated to $\mathbf{Y}$. For example, if the delay operator operates on the sequence $\{x(k)\}_{k=1}^{N}$ (with N indicating the number of samples of the sequence), it transforms the sequence a sample delayed: $q^{-1}\{x(k)\}_{k=2}^{N} = \{x(k)\}_{k=1}^{N-1}$. 'k' is the sample number, normalized with the sample time T. For a state space model with system matrices $(\mathbf{A}_y, \mathbf{B}_y, \mathbf{C}_y, \mathbf{D}_y)$ it holds that the transfer is given by $\mathbf{Y}(q^{-1}) = \mathbf{D}_y + q^{-1}\mathbf{C}_y\left(\mathbf{I}_n - q^{-1}\mathbf{A}_y\right)^{-1}\mathbf{B}_y$ with n the order of $\mathbf{Y}(q^{-1})$ and $\mathbf{I}_n \in \mathbb{R}^{n\times n}$ the identity matrix. Furthermore, matrices, models and systems are denoted by boldface uppercase letters ($\mathbf{X}$), vectors are denoted by boldface lowercase letters ($\mathbf{x}$) and scalar signals are denoted by normal lowercase letters (x). In this paper there is assumed that the set-up is linear time invariant and stationary and that the signals are stationary. Furthermore, in the problem statement and controller design is focussed on the set-up under consideration, which has a scalar reference input, six actuator inputs and six error sensor outputs. The control design in general however, is available for systems with multiple reference inputs, multiple actuator inputs and multiple error sensor outputs. See e.g. [Elliott, 2000].

3.2 Problem statement and controller design

See figure 3 in which a block-diagram of the active vibration isolation control (AVIC) set-up is depicted. Note that from now on explicitly the term AVIC is used, since there is focussed on the active part. $\mathbf{P}$

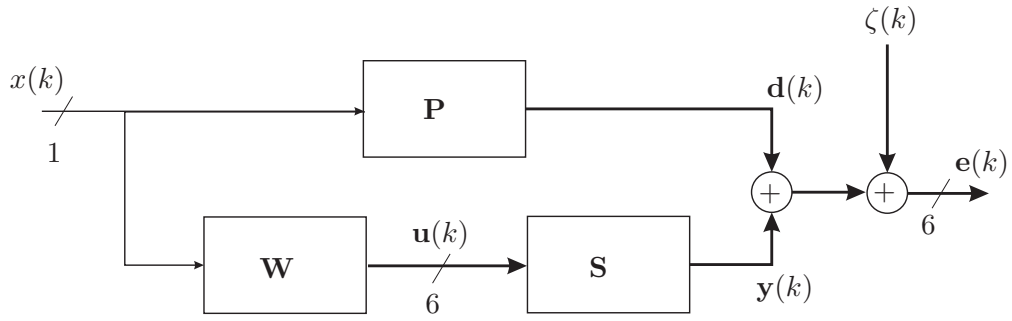

Figure 3: *Block-diagram representing the feedforward AVIC set-up. Signals which enter a plus sign ('+') have the same dimension as signals which leave a plus sign.*

represents the asymptotically stable (which is commonly the case in active noise and vibration control systems [Fraanje, 2004]) single input six output transfer path from the scalar reference input $x(k)$ to the disturbance outputs $\mathbf{d}(k) \in \mathbb{R}^6$ i.e. the primary path (here is chosen for placement of a single vibration exciter, however, in general it is also possible to place multiple vibration exciters and, as such, a single vibration exciter is not a limitation of the design of the 6DOF vibration isolation set-up). For $x(k)$ a zero mean stationary white noise sequence is generated in Matlab Simulink (in practice the reference input(s) are measured by e.g. measurement sensors close to the source). Therefor, the signal $\mathbf{d}(k)$ is given by $\mathbf{d}(k) = \mathbf{P}x(k)$. $\mathbf{S}$ is the asymptotically stable six input six output transfer path from the actuator inputs $\mathbf{u}(k) \in \mathbb{R}^6$ to the anti-disturbance outputs $\mathbf{y}(k) \in \mathbb{R}^6$ i.e. the secondary path. As such, it can be written that $\mathbf{y}(k) = \mathbf{S}\mathbf{u}(k)$. $\zeta(k) \in \mathbb{R}^6$ is the measurement noise, which is statistically independent from the input $x(k)$. The error sensor outputs are given by $\mathbf{e}(k) \in \mathbb{R}^6$ and are a superposition of the disturbance outputs $\mathbf{d}(k)$, the anti-disturbance outputs $\mathbf{y}(k)$ and the measurement noise $\zeta(k)$:

$$\mathbf{e}(k) = \mathbf{d}(k) + \mathbf{y}(k) + \zeta(k).$$

The anti-disturbance outputs $\mathbf{y}(k)$ are generated by the single input six output controller $\mathbf{W}$, which means that: $\mathbf{u}(k) = \mathbf{W}x(k)$. The computation of the controller is done based on minimization of a cost function. Good performance is generally defined in terms of minimizing a H_2 type of cost function [Elliott, 2000]. This can be understood, since that has the physical interpretation of minimizing the power of the error sensor outputs. This results in the following controller design problem.

Problem statement (Controller design problem)**.** *Given the asymptotically stable primary path* $\mathbf{P}$ *and the asymptotically stable secondary path* $\mathbf{S}$*, find an asymptotically stable controller* $\mathbf{W}$ *such that*

$$\mathbf{W} = \arg\min_{\mathbf{W}} J(\mathbf{W}),$$

where the cost function is defined as:

$$J(\mathbf{W}) = \textit{trace}\left\{E\left[\mathbf{e}(k)\mathbf{e}^T(k)\right]\right\} + \textit{trace}\left\{\rho E\left[\mathbf{u}(k)\mathbf{u}^T(k)\right]\right\}. \tag{1}$$

E is the statistical expectation operator [Sayed, 2003]. The term 'trace $\left\{\rho E\left[\mathbf{u}(k)\mathbf{u}^T(k)\right]\right\}$*' in the cost function is control effort weighting which is included to robustify the controller (to e.g. penalize the control effort), with* $\rho \in \mathbb{R}^+$ *a small constant.*

For the solution of this controller design problem, excellent references are available and therefor in this paper only the main results are presented. See for example [Fraanje, 2004, Chapter 2] and [Elliott, 2000, Chapter 5]. The one input six output controller which minimizes the cost-function in equation (1) is given by:

$$\mathbf{W} = -\overline{\mathbf{S}}_o^{-1}\left[\overline{\mathbf{S}}_i^*\overline{\mathbf{P}}\right]_+, \tag{2}$$

with $[\cdot]_+$ the causality operator [Fraanje, 2004] and $[\cdot]^{-1}$ the inverse. $\overline{\mathbf{P}}$ represents the primary path which is augmented due to the regularization factor ρ:

$$\overline{\mathbf{P}} = \begin{bmatrix} \mathbf{P} \\ \\ \mathbf{0}_6 \end{bmatrix},$$

with $\mathbf{0}_6 \in \mathbb{R}^6$ a column vector with zeros. Furthermore

$$\overline{\mathbf{S}} = \overline{\mathbf{S}}_i \overline{\mathbf{S}}_o,$$

represents an inner/outer factorization of the augmented secondary path $\overline{\mathbf{S}}$ [Vidyasagar, 1985; Dewilde and van der Veen, 1998]:

$$\overline{\mathbf{S}} = \begin{bmatrix} \mathbf{S} \\ \sqrt{\rho}\mathbf{I}_6 \end{bmatrix}, \tag{3}$$

with $\sqrt{[\cdot]}$ the square root operation. The six input twelve output inner factor $\overline{\mathbf{S}}_i$ is all-pass which means that:

$$\overline{\mathbf{S}}_i^* \overline{\mathbf{S}}_i = \mathbf{I}_6,$$

with $\overline{\mathbf{S}}_i^*$ the adjoint of $\overline{\mathbf{S}}_i$ [Nijsse, Dijk and Jonker, 2004; Elliott, 2000]. The six input six output outer factor $\overline{\mathbf{S}}_o$ has the property that it has a stable inverse. Note that it holds that

$$\overline{\mathbf{S}}_o^* \overline{\mathbf{S}}_o = \overline{\mathbf{S}}^* \overline{\mathbf{S}} = \mathbf{S}^* \mathbf{S} + \rho \mathbf{I}_6,$$

and that if $\rho = 0$, the controller in equation (2) reduces to the causal Wiener controller [Fraanje, 2004]. Furthermore, note that the controller does not depend on the statistical properties of the measurement noise $\zeta(k)$. That is a well-known result in feedforward control [Elliott, 2000] and straightforward to understand: it is obviously not possible to suppress measurement noise $\zeta(k)$ with a feedforward controller which has no information about the measurement noise. The controller as stated in equation (2) can however not be computed in a practical situation, since the *true* primary path $\mathbf{P}$ and the *true* secondary path $\mathbf{S}$ are not available. Instead, models need to be used; how these models are obtained is explained in the next section. To conclude this section, there is remarked that the control and identification experiments are done on a sample frequency of 2 kHz.

4 Identification of the transfer paths

This section is organized as follows. In section 4.1 the basics of SMI are given. In section 4.2 experimental identification results are presented in brief.

4.1 Subspace Model Identification

See figure 4 which depicts a block-diagram of the transfer paths of the AVIC set-up in figure 3. Assume

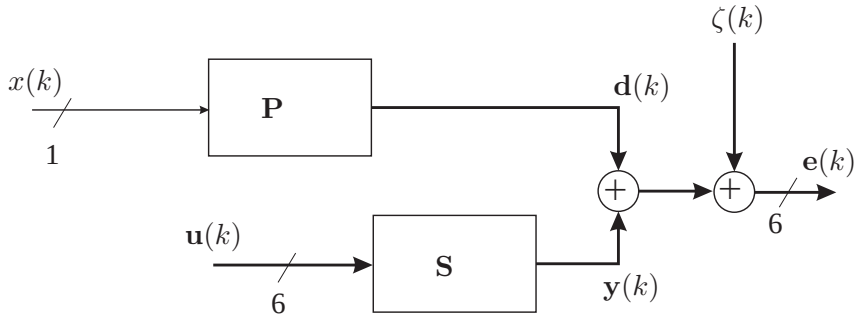

Figure 4: *The two main transfer paths present in the AVIC set-up*

that the input/output relationship from the combined inputs $\widetilde{\mathbf{u}}(k) = \left[x(k)\ \mathbf{u}^T(k)\right]^T$ to the error sensor outputs $\mathbf{e}(k)$ is given by the following state space description (see e.g. [Rugh, 1996] for state space descriptions):

$$\chi \sim \begin{cases} \mathbf{z}(k+1) &= \mathbf{A}\mathbf{z}(k) + \mathbf{B}\widetilde{\mathbf{u}}(k) + \mathbf{w}(k) \\ \mathbf{e}(k) &= \mathbf{C}\mathbf{z}(k) + \mathbf{D}\widetilde{\mathbf{u}}(k) + \mathbf{v}(k) \end{cases}, \tag{4}$$

with $\mathbf{z}(k) \in \mathbb{R}^{N_s}$ the state. The matrices $\mathbf{A}, \mathbf{B}, \mathbf{C}$ and $\mathbf{D}$ have corresponding dimension. $\mathbf{w}(k) \in \mathbb{R}^{N_s}$ and $\mathbf{v}(k) \in \mathbb{R}^6$ are the process noise and measurement noise, respectively. How the process noise $\mathbf{w}(k)$ and measurement noise $\mathbf{v}(k)$ in equation (4) can be 'combined' in the measurement noise $\zeta(k)$ in figure 4 is clarified in [Fraanje, 2004]. The process noise $\mathbf{w}(k)$ and measurement noise $\mathbf{v}(k)$ are assumed to be zero mean stationary white noise sequences, statistically independent from the input $\widetilde{\mathbf{u}}(k)$, with

covariance matrix:

$$\mathrm{E}\left(\begin{bmatrix} \mathbf{v}(k) \\ \mathbf{w}(k) \end{bmatrix} \begin{bmatrix} \mathbf{v}^T(l) & \mathbf{w}^T(l) \end{bmatrix}\right) = \begin{bmatrix} \mathbf{R} & \mathbf{Z} \\ \mathbf{Z}^T & \mathbf{Q} \end{bmatrix} \delta(k-l), \tag{5}$$

where δ is the unit operator which is one for $k = l$ and $[\cdot]^T$ represents the transpose. The matrices $\mathbf{Q}, \mathbf{R}$ and $\mathbf{Z}$ have corresponding dimension. See e.g. [Sayed, 2003, Section 1.3.3] for details on the covariance matrix. The main objective of the identification procedure is to identify the [Haverkamp, 2001; van Overschee and de Moor, 1996]:

1. order N_s of χ;

2. matrices $\mathbf{A}$, $\mathbf{B}$, $\mathbf{C}$ and $\mathbf{D}$ of χ up to a similarity transformation.

The identification of χ is done based on a persistently exciting input/output data-set. Loosely speaking, persistently exciting means that all system dynamics which have to be identified need to be excited. For the identification the Fortran based SLICOT routines are used [NICONET, 2000]. Other software is available however, which implements SMI routines e.g. the standard Matlab system identification toolbox [Ljung, 1999], or the SMI toolbox [Haverkamp et al., 1997]. For the identification there is chosen for the SLICOT routines since they are available as a fast and numerically robust mex-based implementation for Matlab [Redfern and Campbell, 1998].

4.2 Experimental identification results

First the reference input $x(k)$ is excited with a white Gaussian noise sequence and the error sensor outputs $\mathbf{e}(k)$ are recorded. The actuator inputs $\mathbf{u}(k)$ are not excited in this first experiment. Second, the actuator inputs $\mathbf{u}(k)$ are excited with a white Gaussian noise sequence and the error sensor outputs $\mathbf{e}(k)$ are recorded. In this second experiment the reference input $x(k)$ is not excited. The amplifiers of the actuators were set such that the voltages to the actuators were limited to ± 15 Volt. If it is in practice not possible to switch the reference input(s) on and off, but if the reference inputs can be measured, then it

is also possible to estimate the model of the primary path $\mathbf{P}$ and the secondary path $\mathbf{S}$ in one-shot by exciting $\widetilde{\mathbf{u}}(k)$ in one time.

Based on the two separate data-sets, the primary path $\mathbf{P}$ and the secondary path $\mathbf{S}$ are identified separately. For both identification experiments ten seconds of data were used i.e. 20,000 samples. Six seconds of data were used to train the models, while four seconds of data were used to validate the models.

To validate the quality of the model, the Variance-Accounted-For (VAF) measure [Haverkamp, 2001] is used. With the VAF, two matrices $\mathbf{Y} \in \mathbb{R}^{\mathcal{N}\times\mathcal{M}}$ and $\widehat{\mathbf{Y}} \in \mathbb{R}^{\mathcal{N}\times\mathcal{M}}$ can be compared. The VAF is expressed in a percentage (%): the VAF is 100% if the matrices $\mathbf{Y}$ and $\widehat{\mathbf{Y}}$ are identical. If the matrices are not identical the VAF has a value between 0% and 100%. The VAF is defined as:

$$\text{VAF} \;=\; \frac{1}{\mathcal{M}} \sum_{m=1}^{\mathcal{M}} \left[\max \left\{ 1 - \frac{\left|\left| \mathbf{Y}_m - \widehat{\mathbf{Y}}_m \right|\right|_2^2}{||\mathbf{Y}_m||_2^2}, 0 \right\} \times 100\% \right], \tag{6}$$

where 'max' denotes maximum value. The index $m = 1, \ldots, \mathcal{M}$ refers to the m^{th} column of the corresponding matrix. In case of system identification, $\mathbf{Y}$ is the validation output sequence of the system under identification ($\mathcal{N}$ samples tall and $\mathcal{M}$ outputs wide). The validation output sequence $\mathbf{Y}$ is established by 'feeding' the true system with the validation input sequence. The estimate $\widehat{\mathbf{Y}}$ is the estimated validation output sequence which is established by simulating the *model* with the validation input sequence. If the model is perfect, $\widehat{\mathbf{Y}}$ and $\mathbf{Y}$ should be equal and the VAF is 100%. If the model is not perfect $\widehat{\mathbf{Y}}$ and $\mathbf{Y}$ are not equal and the VAF is less then 100 %. The more the VAF differs from 100%, the less accurate the model is. The better the model, the closer the VAF to 100%.

For the primary path a one input six output model of order 100 was identified, which gave a VAF of 99.71% on the validation data. For the secondary path a six input six output model of order 130 was identified, which gave a VAF of 99.82% on the validation data. Since the VAF in both cases is close to 100%, it can be stated the both models are accurate and describe the true system well. One might argue that the model orders are rather high for a set-up consisting of a shaker actuator and six ceramic piezo-

electric actuators. However, the identified model not only comprises the dynamics of the shaker actuator and the ceramic piezo-electric actuators itself, but also amplifiers, reconstruction filters, anti-aliasing filters and so on. Moreover, the set-up consists of a significant number of modes which are excited in the frequency band between 0-1000 Hz.

5 Control experiments

This section is organized as follows. In section 5.1 the simulation results are given, while in section 5.2 the real-time results are presented.

5.1 Simulation experiments in Matlab

We start the derivation by assuming that $\sqrt{\rho} = 0$. Given the models of the primary path and secondary path, the (state space based) controller was computed in equation (2). The causal/anti-causal split was performed in state space using the discrete-time algorithm which was proposed in [Leemhuis, 2004]. A controller was estimated of order 230. The performance of the controller is shown in figure 5 on the fifth error sensor output. The other five error sensor outputs are not shown for brevity. The solid line represents the error sensor output when the controller is switched off, while the dash-dotted line represents the error sensor output when the controller is switched on (we explain the presence of the dotted line later). Approximately below 200 Hz and above 800 Hz the control performance is less then between 200 Hz and 800 Hz. This can be explained by the fact that in the controller the anti-causal part, i.e. $-\overline{\mathbf{S}}_o^{-1}[\overline{\mathbf{S}}_i^*\overline{\mathbf{P}}]_-$, is not incorporated, thereby compromising the performance (with $[\cdot]_-$ the anti-causality operator [Fraanje, 2004]). The anti-causal part originates from the inverted zeros of the secondary path $\mathbf{S}$, which are outside the unit circle [Fraanje, 2004]. In practice, the anti-causal part can never be included in the controller, since it assumes knowledge of future reference inputs, which is not available. As such, the anti-causal part need to be neglected, which is one of the limitations of controller

design [Elliott, 2000]. In table 1 the performance on all six error sensor outputs is stated. The average reduction which is obtained is 12.9 dB. We conclude from figure 5 and table 1 that good performance is

Table 1: *The reduction in dB on the six error sensor outputs in simulation ($\sqrt{\rho} = 0$).*

Sensor 1	**Sensor 2**	**Sensor 3**	**Sensor 4**	**Sensor 5**	**Sensor 6**	**Average**
14.5	14.8	10.9	10.6	12.7	13.6	12.9

obtained. There are however two problems related to the implementation of the estimated controller.

1. The first problem is that the actuator inputs saturate for low frequencies due to a low-frequent high gain of the controller i.e. the controller has a high magnitude for low frequencies (in the lower frequency region, the input is strongly amplified). The low-frequent high gain can be explained by a low-frequent high gain of $\overline{\mathbf{S}}_o^{-1}$ in equation (2). The latter can be explained by the fact that the secondary path has a low-frequent low gain due to the properties of the set-up [Nijsse, 2004]. To prevent actuator saturation, the controller is regularized with a factor $\sqrt{\rho} = 2.65 \cdot 10^{-3}$: this yielded a new controller of order 230.

2. The second problem is that a controller with order 230 could not be implemented on our dSPACE system due to computational limitations. Therefor, controller order reduction was performed with SMI by performing an identification experiment on the controller [Nijsse, 2004; Fraanje et al., 2002]. The order of the controller was reduced from 230 to 135; a controller with order 135 could be implemented. A VAF was obtained of 99.9989% on the reduced order controller, which indicated that the lower order controller was nearly as accurate as its full (higher) order counterpart.

In figure 5 the result is given of the fifth error sensor output in the dotted line with the (regularized reduced order) controller. The controller does not yield performance in the low-frequency area due to the regularization factor $\sqrt{\rho}$. In table 2 the performance on all six error sensor outputs is stated. The

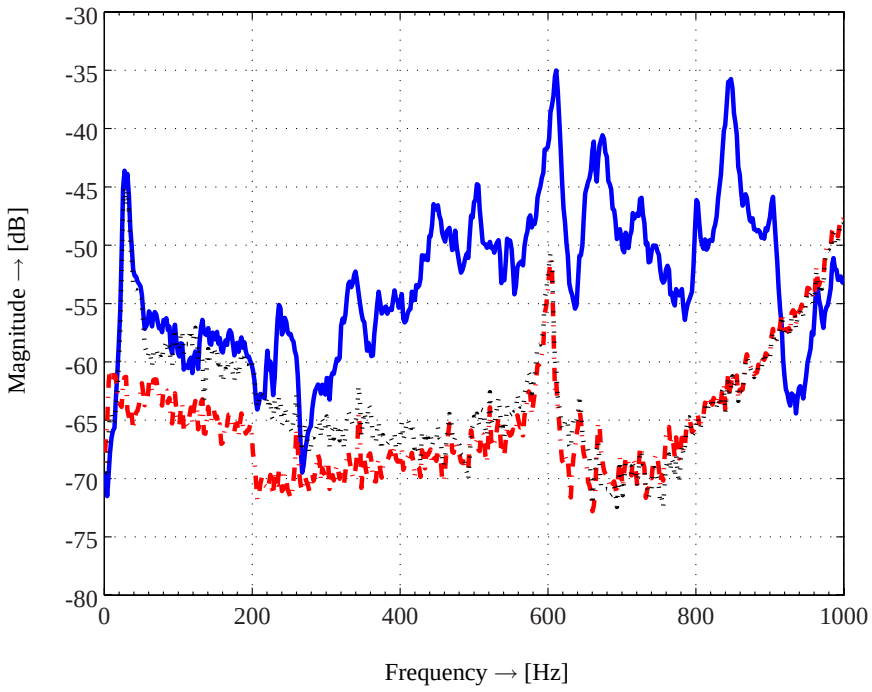

Figure 5: *Performance of the controller in simulation. Spectrum of the fifth error sensor output with no control (solid), with control and* $\sqrt{\rho} = 0$ *(dash-dotted), and with control and* $\sqrt{\rho} = 2.65 \cdot 10^{-3}$ *(dotted).*

average reduction which is obtained over all six error sensor outputs is 11.4 dB, which is 1.5 dB less then the reduction which is obtained without regularization. To further demonstrate the obtained reduction,

Table 2: *The reduction in dB on the six error sensor outputs in simulation (*$\sqrt{\rho} = 2.65 \cdot 10^{-3}$*).*

Sensor 1	**Sensor 2**	**Sensor 3**	**Sensor 4**	**Sensor 5**	**Sensor 6**	**Average**
13.0	13.2	9.6	9.3	10.9	12.3	11.4

in figure 6 the summed error sensor spectra are given (summed over the six sensors), with no and with control.

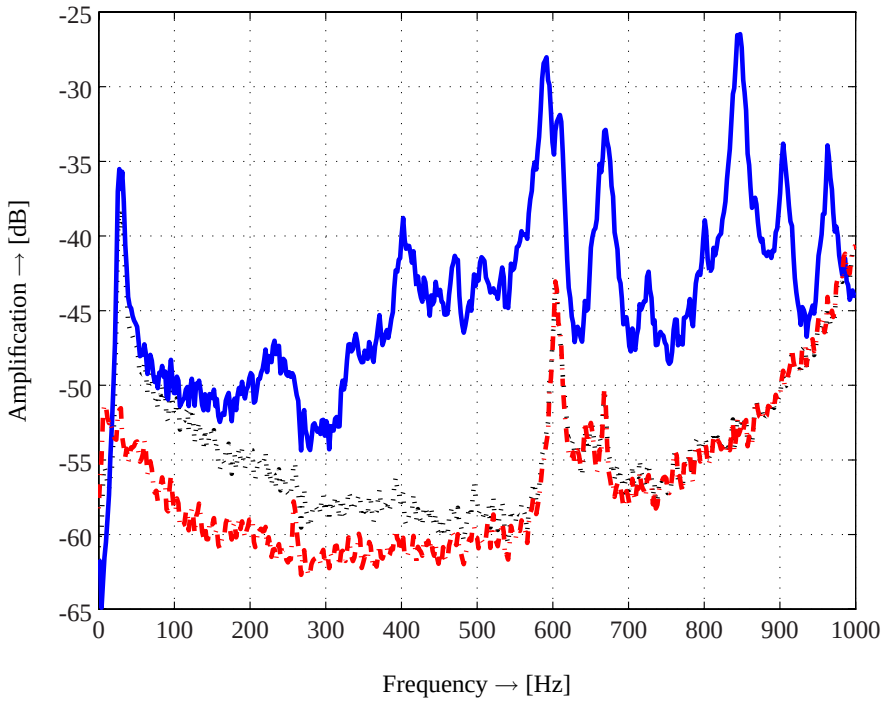

Figure 6: *Performance of the controller in simulation. Summed error sensor output spectra with no control (solid), with control and* $\sqrt{\rho} = 0$ *(dash-dotted), and with control and* $\sqrt{\rho} = 2.65 \cdot 10^{-3}$ *(dotted).*

5.2 Real-time Control Experiments

The (reduced order regularized) controller was also implemented on our real-time dSPACE system. The performance of the controller on the fifth error sensor output is given in figure 7. The solid line in figure 7 can be compared with the solid line in figure 5. The dash-dotted line in figure 7 can be compared with the dotted line in figure 5. In table 3 the performance on all six error sensor outputs is stated. To further

Table 3: *The reduction in dB on the six error sensor outputs in real-time (*$\sqrt{\rho} = 2.65 \cdot 10^{-3}$*).*

Sensor 1	**Sensor 2**	**Sensor 3**	**Sensor 4**	**Sensor 5**	**Sensor 6**	**Average**
9.5	9.7	5.9	6.0	7.4	9.2	8.0

demonstrate the obtained reduction, in figure 6 the summed error sensor spectra are given (summed over

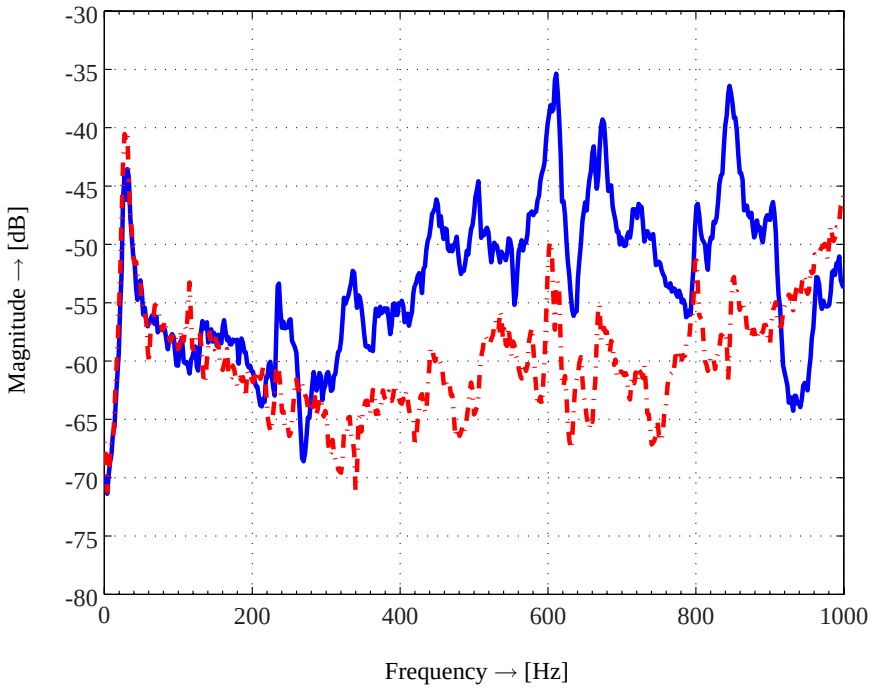

Figure 7: *Performance of the controller in real-time. Spectrum of the fifth error sensor output with no control (solid), and with control and* $\sqrt{\rho} = 2.65 \cdot 10^{-3}$ *(dash-dotted).*

the six sensors), without and with control. Similar to the simulation results, the controller is not active in the low-frequency area due to the regularization. The performance which is obtained in real-time is (obviously) less then the performance which is obtained in simulation. Specifically, an average reduction in real-time is obtained of 8.0 dB as opposed to 11.4 dB in simulation. However, there is concluded that a good performance is obtained in real-time.

One might wonder that, although a reduction in the error sensor outputs was established, what the effect is on transferred vibration energy to the receiver structure. The following can be stated. Due to the design of the construction of the three mounts, the transferred vibration energy can only be passed through the paths with dominant stiffness in which also an actuator is present: in total six paths. All other (parasitic) paths are designed to provide passive isolation. By the AVIC strategy as described, AVIC can be achieved in the dominant paths using six actuator and six sensors. As such, global attenuation is

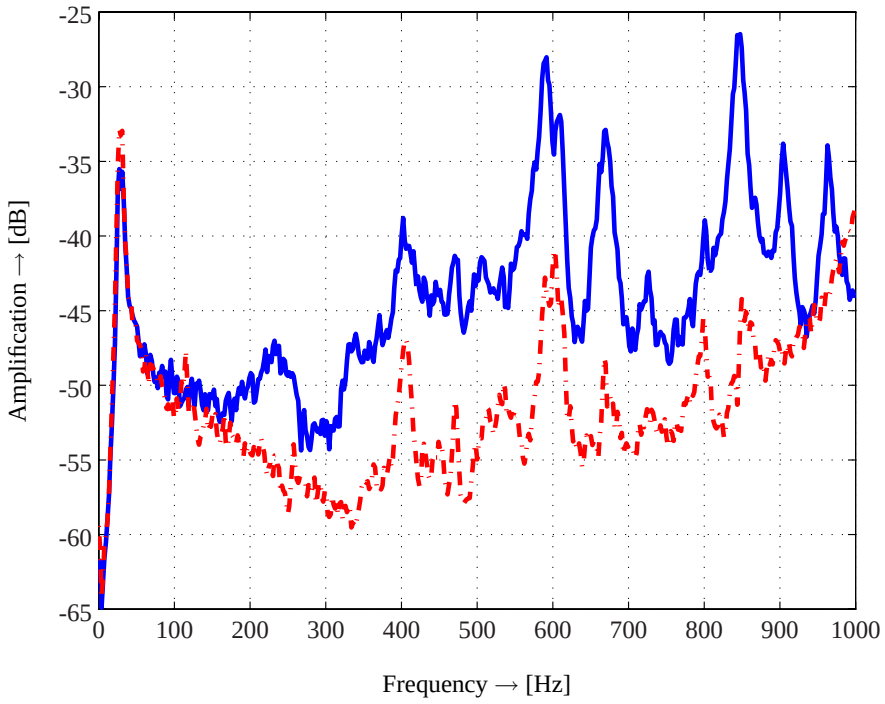

Figure 8: *Performance of the controller in real-time. Summed error sensor output spectra with no control (solid) and with control and* $\sqrt{\rho} = 2.65 \cdot 10^{-3}$ *(dash-dotted).*

achieved.

6 Conclusions

In this paper a novel hybrid vibration isolation approach was introduced which uses a combination of passive and active vibration control techniques to provide additional design freedom. The approach can be used to meet higher design requirements with respect to vibration isolation. To illustrate the feasibility of the approach, a stiff hybrid six-degrees-of-freedom vibration isolation set-up was presented.The paper reported successful experiments which were performed on the six-degrees-of-freedom vibration isolation set-up and demonstrated that the transfer paths of the set-up could be accurately modelled by linear state space models of which the parameters were obtained by subspace model identification. Furthermore a fixed gain H_2 controller was designed, implemented and validated which was able to reject broadband

disturbances up to 1 kHz in the error sensor outputs with an average reduction of 11.4 dB in simulation and 8.0 dB in real-time.

References

A. Abu Hanieh, M. H. and Preumont, A.: 1999, Stiff and soft stewart platforms for active damping and active isolation of vibrations, *ACTUATOR 2002 - 8th International Conference on New Actuators*, Bremen, Germany.

Dewilde, P. and van der Veen, A.-J.: 1998, *Time-varying systems and computations*, Kluwer Academic Publishers.

Elliott, S.: 2000, *Signal processing for active control*, Academic Press.

Fraanje, P.: 2004, *Robust and fast schemes in active noise and vibration control*, PhD thesis, University of Twente, P.O. Box 217, 7500 AE, Enschede, The Netherlands.

Fraanje, R., Verhaegen, M., Berkhoff, A. and Doelman, N.: 2002, Mimo H_2 and robust feedback controller estimation for a vibrating plate using subspace model identification, *ACTIVE 2002: The 2002 International Symposium on Active Control of Sound and Vibration*, Southamption, UK, pp. 1251–1262.

Fukuda, T. and Tzou, H. (eds): 2002, *Precision sensors, actuators and systems*, number 17 in *Solid Mechanics and Its Applications*, Kluwer Academic Publishers.

Fuller, C., Elliott, S. and Nelson, P.: 1996, *Active control of vibration*, Academic Press Limited.

Hansen, C. and Snyder, S.: 1997, *Active control of noise and vibration*, E & FN Spon.

Haverkamp, B., Chou, C. and Verhaegen, M.: 1997, SMI toolbox: A matlab toolbox for state space model identification, *Journal A* **38**(3), 34–37.

Haverkamp, L.: 2001, *State space identification*, PhD thesis, Delft University of Technology, Delft, The Netherlands.

Horodinca, M., Hanieh, A. A. and Preumont, A.: 2002, A soft six degrees of freedom active vibration isolator based on a stewart platform, *ACTIVE 2002: The 2002 International Symposium on Active Control of Sound and Vibration*, ISVR, Southampton, UK, pp. 1021–1032.

Kuo, S. and Morgan, D.: 1996, *Active noise control systems*, John Wiley & Sons, Inc.

Leemhuis, A.: 2004, *Design of the causal wiener controller for active vibration isolation control: a state space approach*, Master's thesis, University of Twente, Faculty of Engineering Technology, Department of Mechanical Engineering, Laboratory of Mechanical Automation.

Ljung, L.: 1999, *System identification*, Prentice Hall, Inc.

Mead, D. J.: 1998, *Passive vibration control*, John Wiley and Sons.

NICONET, I. S.: 2000, The SLICOT package - task III.A: Development of standard software for linear, time-invariant state space model identification. Katholieke Universiteit Leuven, Department of Electrical Engineering, Kasteelpark Arenberg 10, 3001, Leuven-Heverlee, Belgium.

Nijsse, G.: 2004, *Design, implementation and validation algorithms for active vibration isolation control*, PhD thesis, To be published, University of Twente, Faculty of Engineering Technology, Department of Mechanical Engineering, Mechanical Automation Laboratory, P.O. Box 217, 7500 AE, Enschede, The Netherlands.

Nijsse, G., Dijk, J. V. and Jonker, J.: 2004, Feedback control of broadband disturbances on a one-degree-of-freedom vibration isolation set-up, *ISMA2004: International Conference on Noise and Vibration Engineering*, Leuven, Belgium.

Nijsse, G., Super, H., Dijk, J. V. and Jonker, J.: 2004, Feedforward control of broadband disturbances on a six-degrees-of-freedom vibration isolation set-up, *ACTIVE 2004: The 2004 International Symposium on Active Control of Sound and Vibration*, Williamsburg, Virginia, USA.

Nijsse, G., Verhaegen, M., Schutter, B. D., Westwick, D. and Doelman, N.: 1999, State space modeling in multichannel active control systems, *ACTIVE 99: The 1999 International Symposium on Active Control of Sound and Vibration*, Fort Lauderdale, Florida, USA, pp. 909–920.

Redfern, D. and Campbell, C.: 1998, *The MATLAB 5 handbook*, Springer Verlag.

Rugh, W. J.: 1996, *Linear system theory*, second edn, Prentice Hall, Inc.

Sayed, A. H.: 2003, *Fundamentals of adaptive filtering*, John Wiley & Sons.

Super, H., Nijsse, G., Dijk, J. V. and Jonker, J.: 2004, Design of a six-degrees-of-freedom vibration isolation set-up, *ACTIVE 2004: The 2004 International Symposium on Active Control of Sound and Vibration*, Williamsburg, Virginia, USA.

Thoeni, U.: 1994, *Programming real-time multicomputers for signal processing*, International Series in Acoustics, Speech and Signal Processing, Prentice Hall, Inc.

van Overschee, P. and de Moor, B.: 1996, *Subspace identification for linear systems*, Kluwer Academic Publishers.

Verhaegen, M.: 1994, Identification of the deterministic part of MIMO state space models given in innovations form from input-output data, *Automatica* **30**(1), 61–74.

Vidyasagar, M.: 1985, *Control system synthesis: a factorization approach*, MIT Press.